Electronic Supplementary Material (ESI) for Soft Matter
This journal is © The Royal Society of Chemistry 2020

Penetration and preferential binding of charged nanoparticles to mixed lipid monolayers: interplay of lipid packing and charge density

Anurag Chaudhury[a], Koushik Debnath[b], Wei Bu[c], Nikhil R. Jana[b] and Jaydeep Kumar Basu[a]‡

[a] *Department of Physics, Indian Institute of Science, Bangalore 560012, India.*

[b] *School of Materials Science, Indian Association for the Cultivation of Science, Kolkata-700032, India.*

[c] *NSF's ChemMatCars, University of Chicago, Argonne National Lab, Lemont, IL 60439 USA.*

‡*basu@iisc.ac.in*

Nanoparticle characterization data:

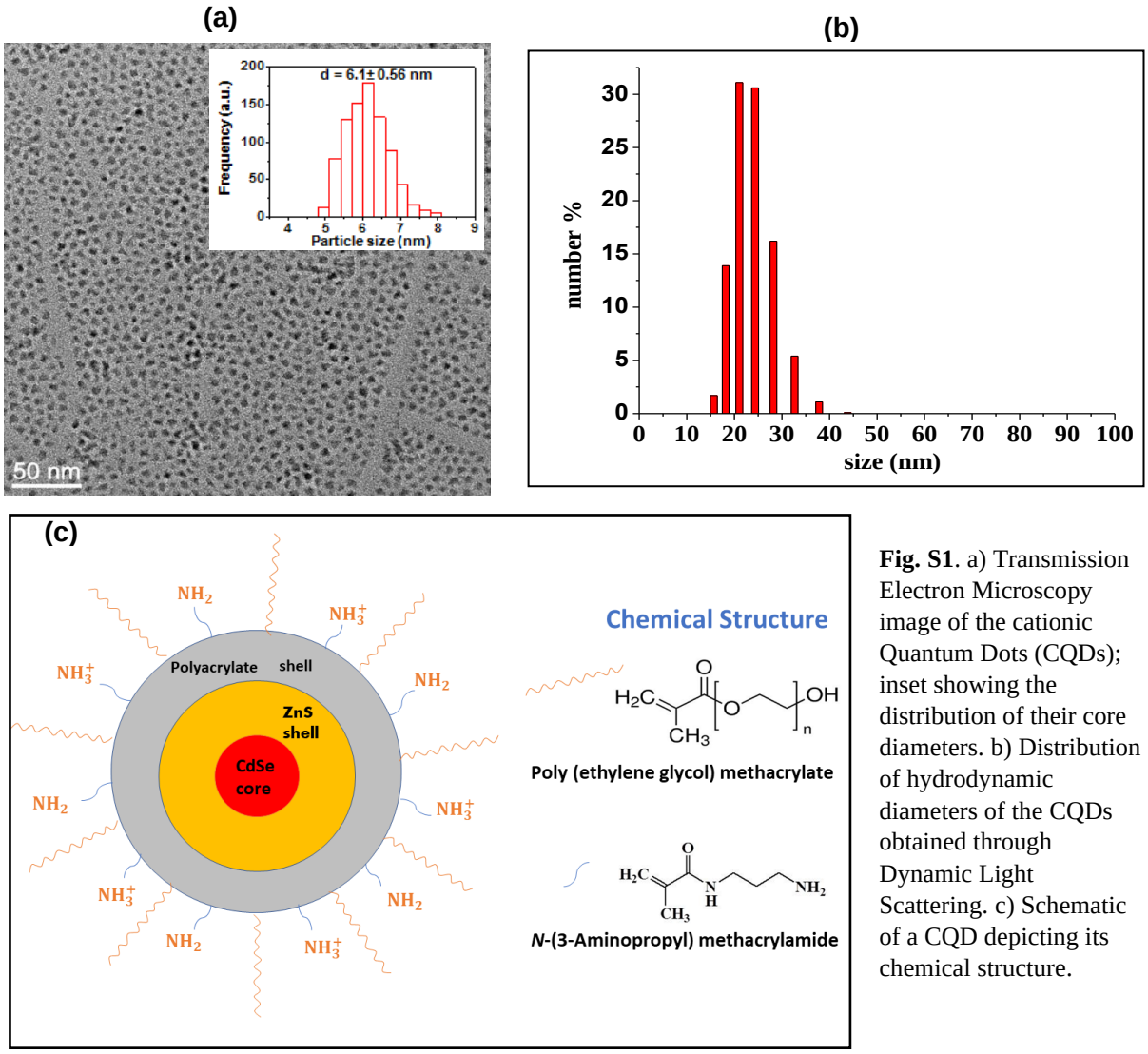

Fig. S1. a) Transmission Electron Microscopy image of the cationic Quantum Dots (CQDs); inset showing the distribution of their core diameters. b) Distribution of hydrodynamic diameters of the CQDs obtained through Dynamic Light Scattering. c) Schematic of a CQD depicting its chemical structure.

Red emissive Quantum dots having CdSe core and ZnS shell have been synthesized by previously reported method.[1,2] First, CdSe nanocrystals were synthesized in octadecane solution at 280°C followed by the ZnS shelling on these nanoparticles at 200 °C. These hydrophobic QDs were coated with N-(3-aminopropyl)methacrylamide, poly (ethyleneglycol)methacrylate and bis[2-(methacryloyloxy)ethyl] phosphate as acrylate monomers. to make them hydrophilic. Further, these quantum dots were characterized for their hydrodynamic diameter and zeta potential by a Brookhaven 90 Plus size and zeta potential analyzer which were found to be 21 nm and +18mV respectively at pH 7. N-(3-aminopropyl)methacrylamide has amine functional groups, thus after the protonation these functional groups provide higher positive charge to the QDs at pH lower pH. The Trasmission Eleectron Microscopy image of the QDs reveal a core diameter of 6.1 ± 0.6 nm.

Table 1. Zeta potential of the cationic QDs in different pH solvents

pH	Surface potential (mV)
4.5	**+60**
6	**+35**
7	**+18**
10	**-1**

X-ray Fluorescence (XRF) data:

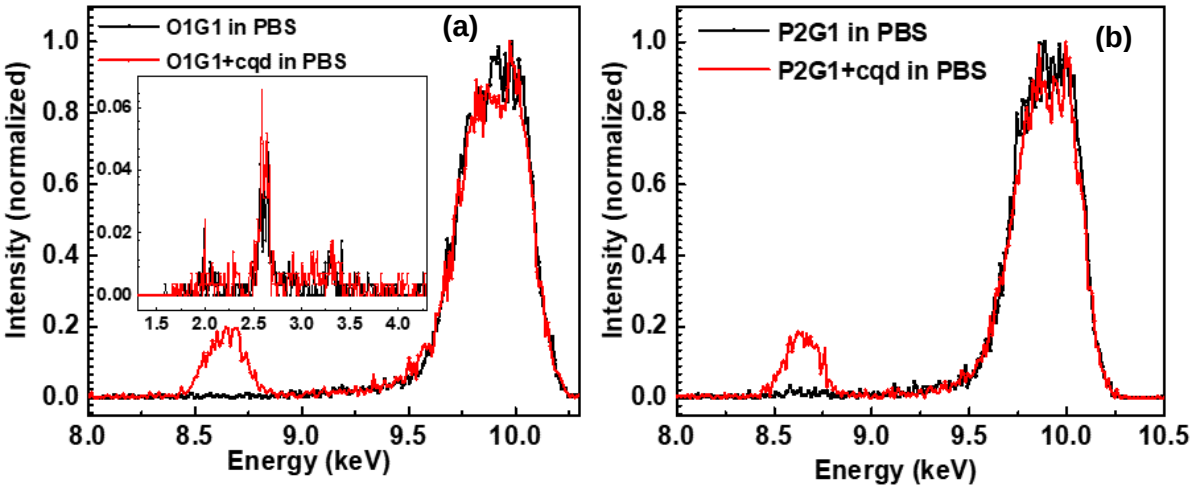

Fig. S2. a) shows XRF data taken from pristine O1G1 FLM (black) and O1G1+cqd data (red) in GID geometry; inset shows zoomed-in XRF to highlight the 2.6 keV Chlorine peak, 2 keV Phosphorus peak and 3.3 keV Potassium peak; and b) shows XRF data taken from pristine P2G1 (black) and P2G1+cqd data (red) in GID geometry.

The Zinc X-ray fluorescence peak at 8.6 keV in Fig. S2a confirms the presence of CQDs bound to the O1G1 monolayer in PBS subphase. The inset showing the Chlorine, Phosphorus and Potassium peaks indicate the presence of counterionic layer beneath the FLM which has a significant effect on the binding nature of the CQDs as discussed in the main manuscript. The presence of the CQD binding to the P2G1 monolayer was also confirmed from the Zn XRF peak (Fig. S2b)

Competing models for Reflectivity Data:

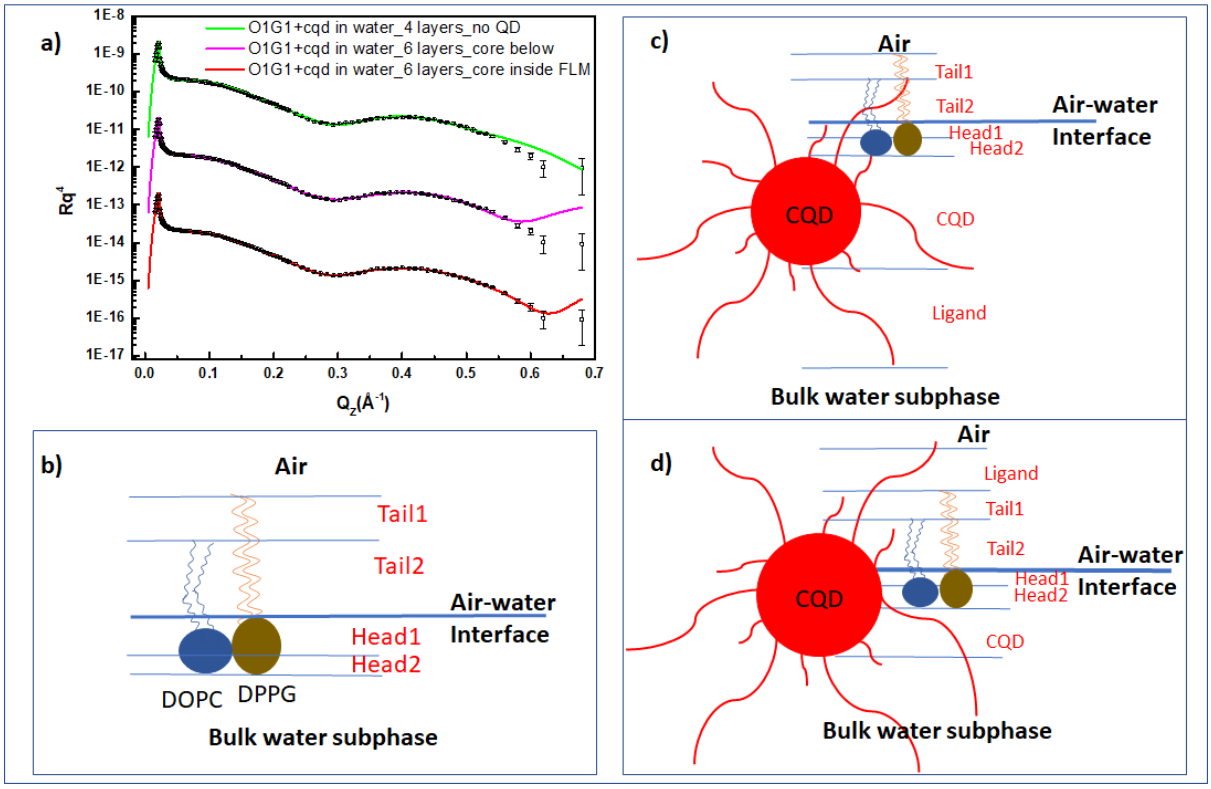

Fig. S3. a) XR data of DOPC:DPPG(1:1)/O1G1 after adding CQDs on DI water subphase. The green solid line shows fit to the O1G1+cqd data with 4 layers assuming there is no CQD layer beneath, the magenta line shows fit to the data considering the entire CQD core lies just below the floating lipid monolayer (FLM) and the red solid line is the best fit to the O1G1+cqd data with 6 layers assuming the CQD has penetrated the FLM. Schematics in b), c) and d) illustrate the models adopted to fit the data with the green, magenta and red lines in a) respectively.

The normalized reflectivity data obtained from O1G1 free lipid monolayer (FLM) on DI water subphase (pH 6) after 10nM CQD incubation was fit with different models (ESI Fig. S2). The green solid line shows the fit considering there is no CQD layer beneath the FLM (Fig. S2b schematic), but the fit was poor, yielding a χ^2 value of 47.66. Another competing model considering the CQD core below the FLM (Fig. S2c schematic) was allowed to fit the data. The fit (magenta solid line) significantly improved providing a χ^2 value of 13.87. However, the best fit (red solid line) was obtained when the system was modelled with the CQD core penetrating the film (Fig. S2d schematic), producing a χ^2 value of 9.13. An additional Ligand layer on top of the FLM was needed to fit the fit the data. This layer was contrasting enough as compared to air to be detected by the X-rays. But because of low CQD coverage, the Ligand layer below the CQD core layer was not contrasting enough in the DI water subphase to be detected as a separate layer.

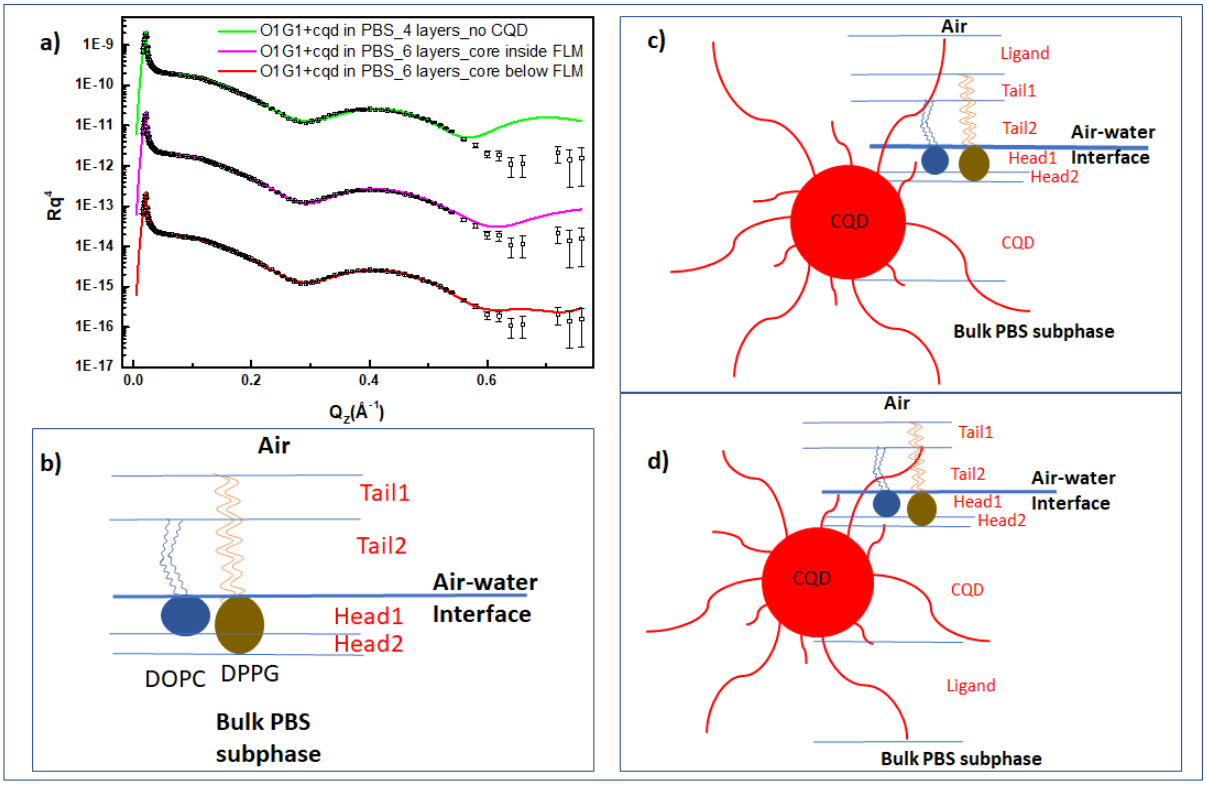

Fig. S4. a) XR data of DOPC:DPPG(1:1)/O1G1 after adding CQDs on PBS subphase. The green solid line shows fit to the O1G1+cqd data with 4 layers assuming there is no CQD layer beneath, the magenta line shows fit to the data considering the CQD core penetrates the floating lipid monolayer (FLM) and the red solid line is the best fit to the O1G1+cqd data with 6 layers assuming the CQD core lies just below the FLM. Schematics in b), c) and d) illustrate the models adopted to fit the data with the green, magenta and red lines in a) respectively.

The normalized reflectivity data obtained from O1G1 free lipid monolayer (FLM) on PBS subphase (pH 7) after 10nM CQD incubation was fit with different models (ESI Fig. S3). The green solid line shows the fit considering there is no CQD layer beneath the FLM (Fig. S3b schematic), but the fit was poor, yielding a χ^2 value of 176.94, and pertaining to the need of a CQD layer. Thus, a competing model considering the CQD core penetrating the FLM (Fig. S3c

schematic), similar to the best fit model for O1G1 +CQD on DI water, was allowed to fit the data. The fit (magenta solid line) significantly improved, giving a χ^2 value of 87.21. But it was still not the best fit. The best fit (red solid line) was obtained when the system was modelled with the CQD core below the film (Fig. 3d schematic), producing a χ^2 value of 29.08. Because of higher CQD coverage than on DI water subphase, here an additional Ligand layer below the FLM was needed to fit the fit the data.

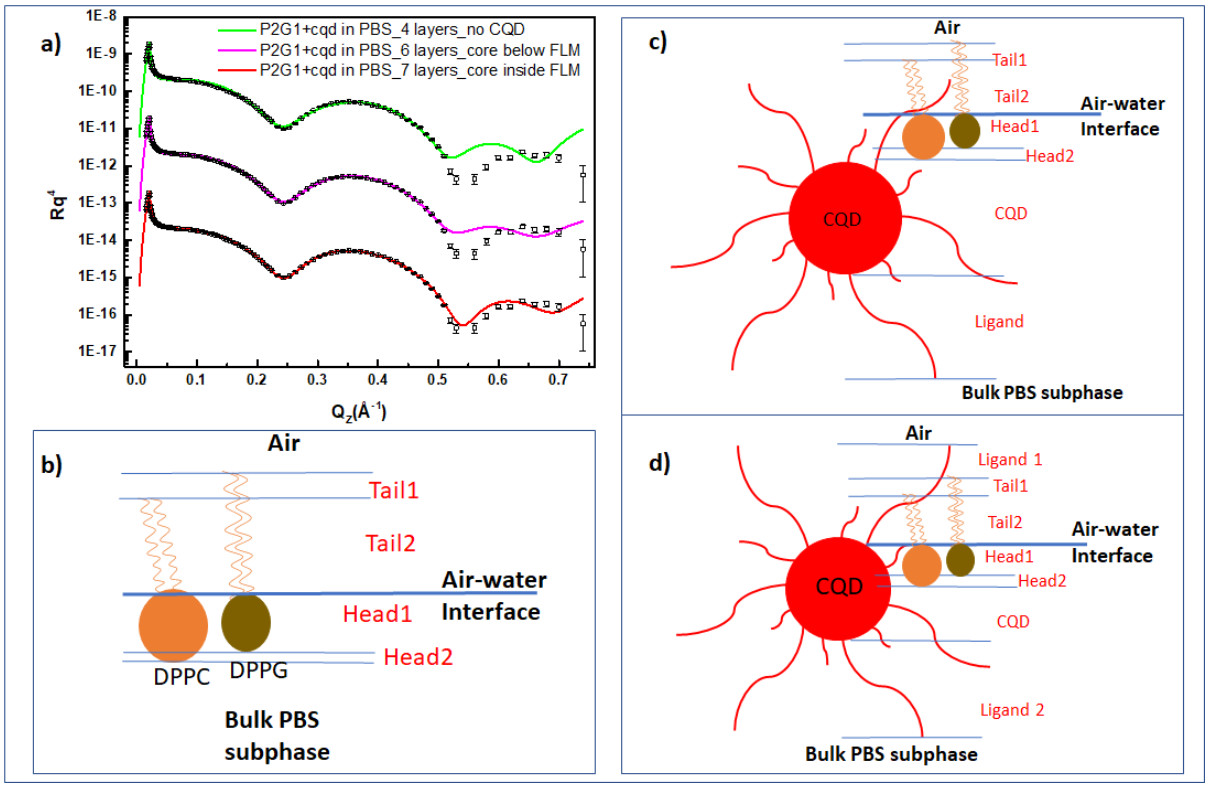

Fig. S5. a) XR data of DPPC:DPPG(2:1)/O1G1 after adding CQDs on PBS subphase. The green solid line shows fit to the P2G1+cqd data with 4 layers assuming there is no CQD layer beneath, the magenta line shows fit to the data considering the entire CQD core lies just below the FLM and the red solid line is the best fit to the O1G1+cqd data with 7 layers assuming the CQD has penetrated the FLM. Schematics in b), c) and d) illustrate the models adopted to fit the data with the green, magenta and red lines in a) respectively.

The normalized reflectivity data obtained from P2G1 free lipid monolayer (FLM) on PBS subphase (pH 7) after 10nM CQD incubation was fit with different models (ESI Fig. S4). The X-rays were sensitive to the presence of a CQD layer because a model considering no CQD layer (Fig. S4b schematic) could not fit (green solid line) the data well, giving a high χ^2 value of 286.16. Thus, a competing model considering the CQD core below the FLM (Fig. S4c schematic) was allowed to fit the data. The fit (magenta solid line) significantly improved, giving a χ^2 value of 49.06. But it was still not the best fit. The best fit (red solid line) was obtained when the system was modelled with the CQD core penetrating the film (Fig. S4d schematic), producing a χ^2 value of 16.6. Apart from the need of a fractional coverage low-density Ligand layer above the FLM (due to penetration of the CQDs), another ligand layer below the CQD core was necessary to fit the data, resulting in a 7-layered model. This is

because this system had the highest CQD coverage out of the 3 monolayers studied, due to which the X-rays could sensitively detect the presence of a high SLD ligand layer in the background of the bulk PBS subphase.

Isotherm Data:

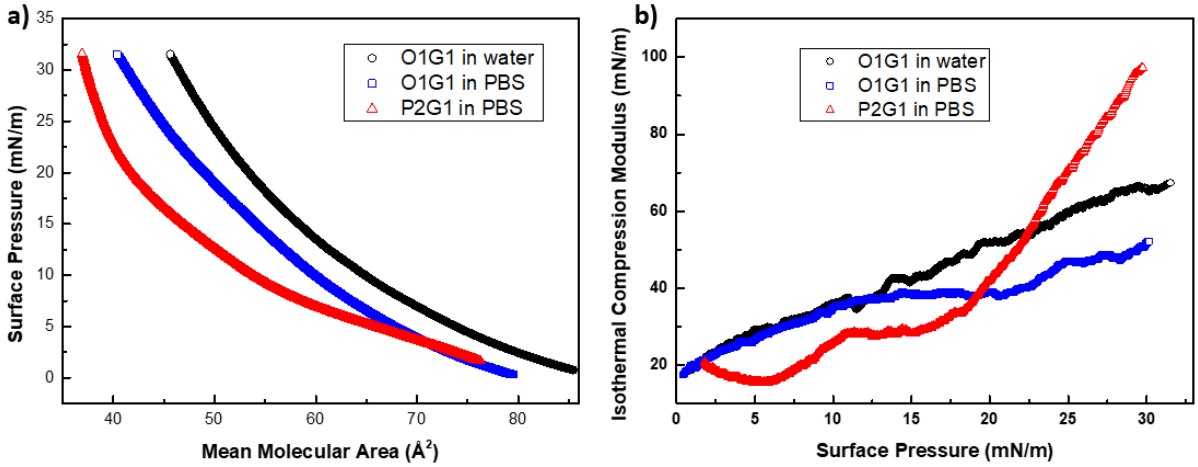

Fig. S6. a) Isotherms and b) Isothermal Compression moduli of O1G1 in DI water and PBS subphase, and of P2G1 on PBS subphase, indicating that P2G1 is a more rigid monolayer than O1G1.

The isotherm data were collected in the manner described in the Methods section of the article. The FLMs were compressed and expanded once before the final compression, in order to form a homogeneous film at the air-water interface. The isotherms suggest that the average mean molecular area of the mixed FLMs is the smallest in case of P2G1. The moduli values also reveal that P2G1 is the most rigid monolayer out of the 3 systems.

Fluorescence Microscopy measurements:

For these experiments, a KVS Nima Langmuir trough having a area of 243 cm^2 was placed above an objective in an inverted microscope arrangement, part of Leica Microsystems. An optical window was made at the base of the trough to allow the LASER beam to illuminate the Atto 647N tagged lipids floating at the air-water interface. Stock solutions of the individual lipids were prepared in chloroform and aliquots of these lipid stocks were mixed to prepare O1G1 and P2G1 solutions, which were spread on the PBS subphase. One cycle of compression and expansion of the barriers were performed to homogenize the floating mixed lipid monolayer. Fluorescence images were captured in the final compression at various pressures. CQDs were added into the subphase in the same fashion as described in the Methods Section of the manuscript by allowing the barriers to hold the film at a constant surface pressure. Images were captured before and after adding the CQDs.

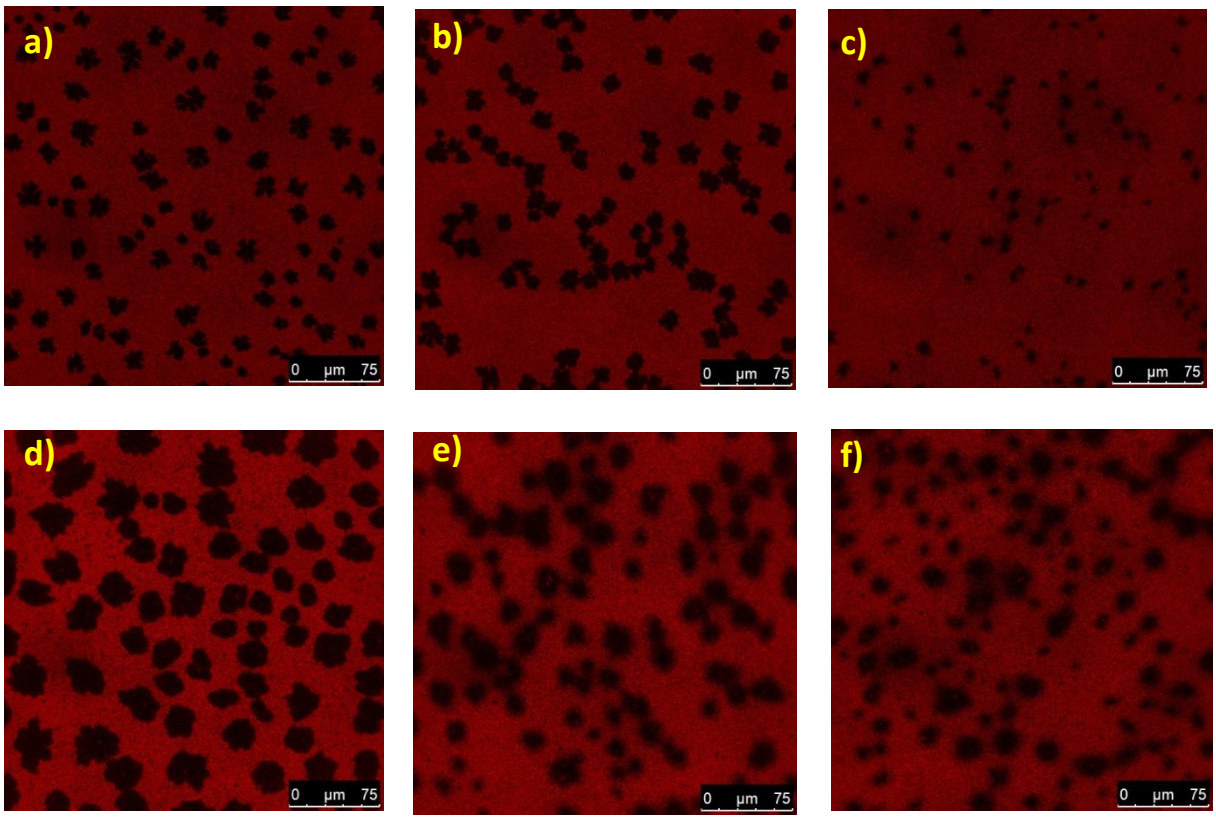

Fig. S7. Confocal images of a) pristine O1G1 floating monolayer at 32 mN/m, and after b) 14 min and c) 15 min of 20nM CQD incubation into the PBS subphase. The dye-devoid regions are the DPPG domains. The CQDs seem to reduce the line tension at the domain boundaries and rupture the domains and seem to infiltrate the DPPG lipids and cause them to diffuse into the disordered DOPC (dye-rich) domains. Confocal images of d) pristine P2G1 floating monolayer at 26 mN/m and after e) 6 min and f) 16 min of 6 nM CQD addition into PBS subphase. Here, the dye-devoid regions are the DPPC domains. The CQDs seem to reduce the line tension at the domain boundaries and rupture the domains but result in comparatively less domain changes due to highly ordered lipid components.

The fluorescence microscopy images collected from the O1G1 monolayer before and after adding CQDs reveal that the ordered DPPG domains (dye-devoid) seem to coalesce after addition of the CQDs till the 14^{th} minute of incubation. Thereafter, the shrinkage of domains were observed suggesting that the CQDs try to reduce the line tension between the domain boundaries causing the DPPG lipids in the domain boundaries to diffuse out into the fluidic DOPC disordered phase. Such reduction in domain size was also observed in P2G1 after CQD incubation, but the extent of DPPC domain (dye-devoid regions) is not pronounced in this case. This indicates that the CQDs effect on the DPPC lipids in P2G1 is comparatively less as compared to the DPPG domains in O1G1. These P2G1 domains getting less affected can be attributed to the highly rigid P2G1 monolayer as seen from the Isothermal data.

GID supporting data:

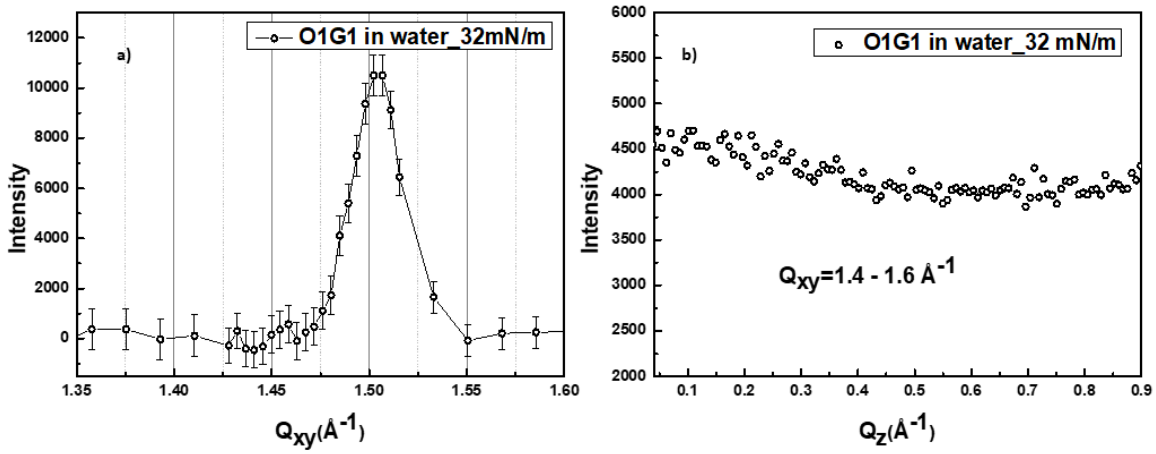

Fig. S8. a) GID data of DOPC:DPPG(1:1)/O1G1 on DI water subphase at 32mN/m; b) Bragg rod of the Bragg peak in a) integrated from Q_{xy} = 1.4 – 1.6 Å^{-1}, smoothened and data density reduced using 5 point Adjacent-Averaging. The Bragg peak is along the [0 2] lattice vector of the centred-rectangular lattice which peaks at Q_z = 0 Å^{-1} as evident from b).

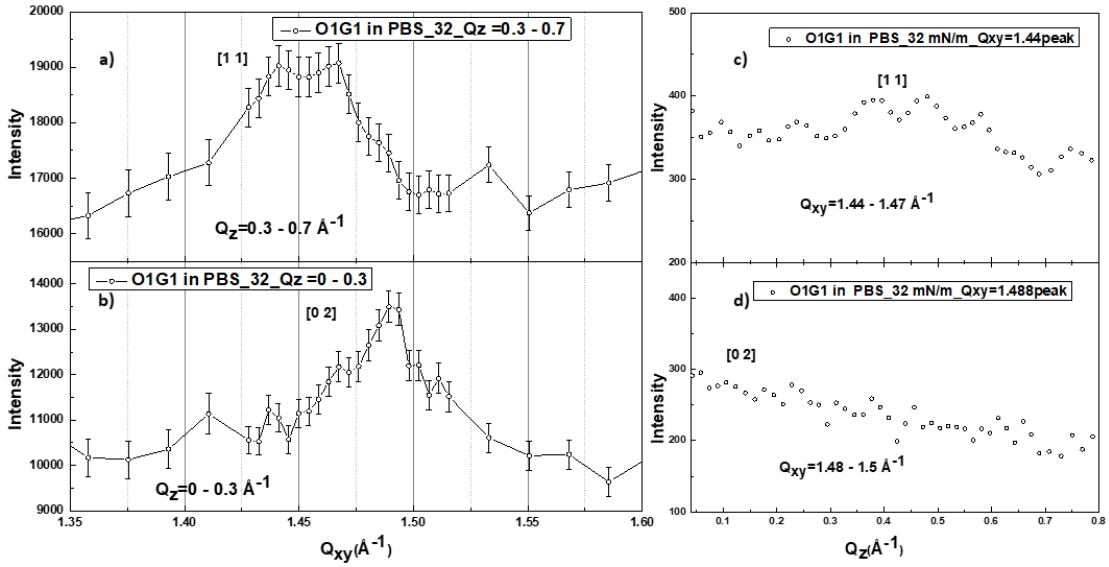

Fig. S9. Bragg peaks of O1G1 on PBS subphase at 32mN/m along the a) [1 1] and b) [0 2] lattice vectors, integrated through different Q_Z regions as indicated in the graphs. Their corresponding Bragg rod profiles are shown in c) and d) which have been integrated through different Q_{xy} regions (as indicated in the graphs) and smoothened using 30point Adjacent-Averaging after masking the bad data points and data density reduced to 1in 10 points. The [1 1] Bragg peak is very wide with an indication of a second peak along [1 1], signifying that in PBS subphase, the DPPG lattice is distorted (from ideal hexagonal) and there are sublattices which are contributing to the [1 1] Bragg peak intensities.

The GID data collected from O1G1 monolayer on DI water subphase at 20^{0}C at a surface pressure of 32 mN/m as shown in Fig. S7 produce only one Bragg peak, indicating that the ordered DPPG lipids form undistorted hexagonal lattices with no azimuthal tilt away from their nearest neighbours in the lattice.

The GID data collected from the O1G1 FLM on PBS subphase at 20^0C at a surface pressure of 32 mN/m as shown in Fig. S8 shows that there are two Bragg peaks. The one at Q_z=0 $Å^{-1}$ corresponds to the [0 2] Bragg reflection. The binned GID plot in the range Qz=0.3 to 0.7 $Å^{-1}$ (Fig. S8a) shows that the presence more than 1 peak. It implies that in contrast to the FLM on DI water, here the DPPG molecules form distorted hexagonal lattices. There may be the possibility of the presence of sublattices having different lattice parameters.

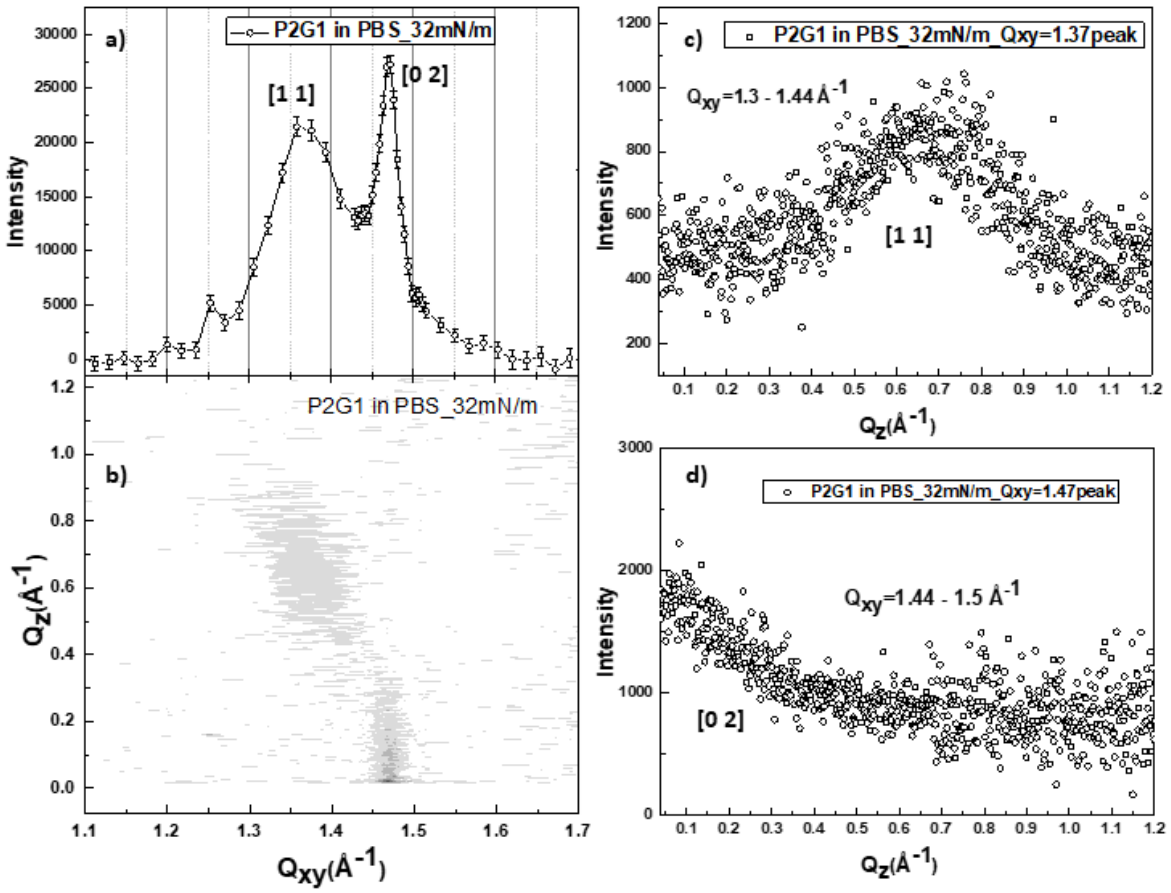

Fig. S10. a) Bragg peaks of DPPC:DPPG(2:1)/P2G1 on PBS subphase at 32mN/m along the [1 1] and b) [0 2] lattice vectors, integrated throughout Q_Z space of the 2-D GID Intensity contour map in Q space as indicated in b).Their corresponding Bragg rod profiles are shown in c) and d) which have been integrated through different Q_{xy} regions as indicated in the graphs.

The GID data of P2G1 monolayer collected at 32 mN/m are much similar to the data collected from the same FLM at 26 mN/m; the [0 2] and [1 1] Bragg peaks are slightly shifted towards higher Q_{xy} at 32 mN/m (comparing with the data shown in the main article), implying that the corresponding lattice is more compact than the one at 26 mN/m. The [1 1] peak is a result of diffraction from the DPPC grains, while the [0 2] peak arises due to the diffraction from both the DPPC and the DPPG lattices.

The Bragg peaks of O1G1 FLM on DI water at 26 mN/m collected before and after addition of the CQDs are shown in the main article. Fig. S10 illustrates the Bragg rods of the corresponding Bragg peaks. The [1 1] Bragg rods shifting towards higher Q_z after CQD

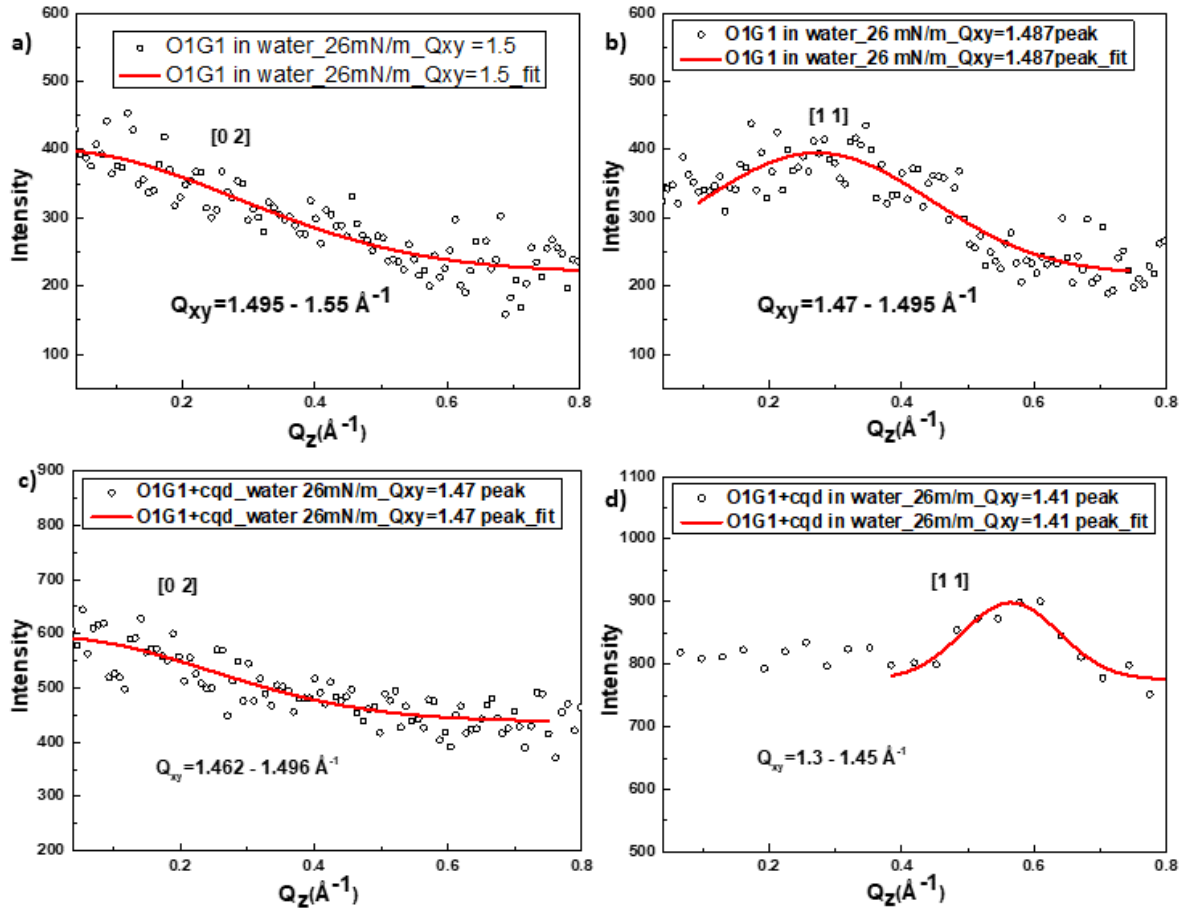

Fig. S11. a) [0 2] and b) [1 1] Bragg rod profiles of pristine O1G1 in DI water; c) [0 2] and d) [1 1] Bragg rod profiles of O1G1 after CQD binding. The rods have been integrated through different Q_{xy} regions as indicated in the graphs and smoothened using 5point Adjacent-Averaging after masking the bad data points and data density reduced to 1 in 5 points, except for d) which has been smoothened using 20point Adjacent-Averaging and data reduced to 1 in 20 points to enhance the signal to noise ratio.

addition is a clear sign that the azimuthal angle of the DPPG tails tilting further away from the nearest neighbours. Also, the FWHM of the [1 1] rod is much small, producing a large out-of-plane coherence length which may be due to the presence of the CQD ligands above the FLM due to high penetration of the CQDs, as discussed in the article.

Fig. S11 shows the GID data collected from the O1G1 FLM on PBS subphase at 20^0C at a surface pressure of 26 mN/m. The monolayer produces 2 Bragg peaks, one at Q_z=0 $Å^{-1}$ corresponding to the [0 2] Bragg reflection (Fig. S11a,b) and second, the [1 1] peak located at higher Qz (Fig. 11a,c). It pertains to a centred-rectangular lattice whose lattice parameters are listed out in Table 3 of the main article. After CQD addition, the Bragg peaks shift towards lower Q_{xy} values (Fig. 11d) indicating lattice expansion. Similar to that on DI water subphase, even on PBS subphase the [1 1] Bragg rod shifts towards higher Q_z (Fig. 11f) implying that the tilt angles (azimuth) have increased after CQD binding. However, unlike the case on DI water,

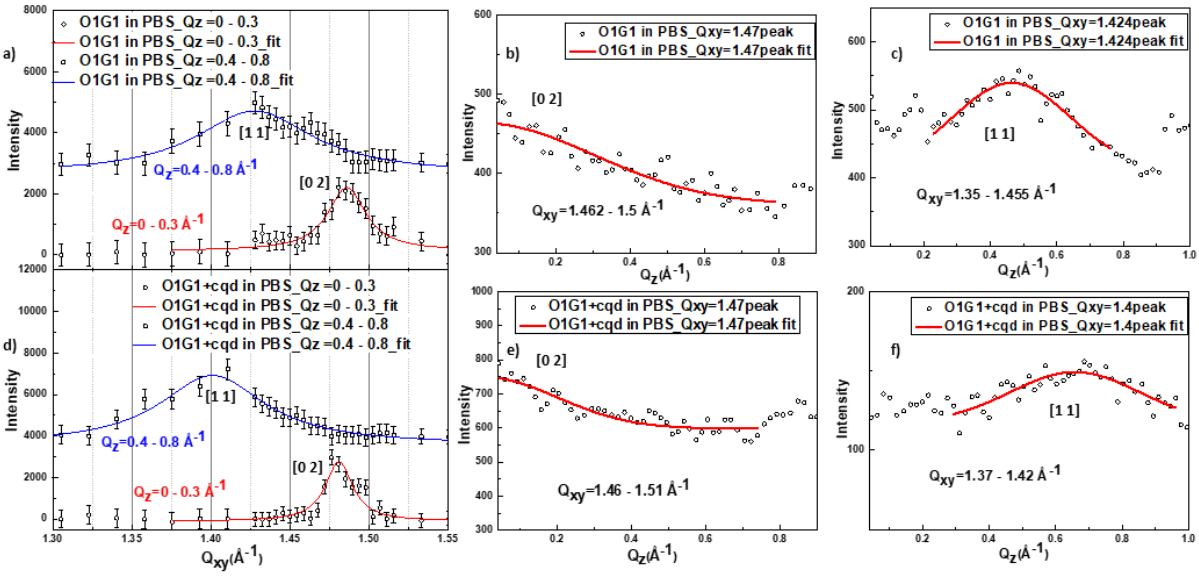

Fig. S12. a) Bragg peaks of O1G1 on PBS subphase at 26 mN/m along the [1 1] and [0 2] lattice vectors, integrated through different Q_Z regions as indicated in the graphs. Their corresponding Bragg rod profiles are shown in b) and c) which have been integrated through different Q_{xy} regions as indicated in the graphs and smoothened using 20point Adjacent-Averaging after masking the bad data points. The same data for the monolayer after CQD addition is shown in the lower panel figures d), e) and f). The slight shift in the [1 1] Bragg peak towards left in d) indicates the DPPG lattice tried to expand to accommodate the CQD ligand infiltration. The [1 1] rod in f) also shifted towards higher Q_z indicating an increase in tilt angles of the DPPG rods. The values have been listed in the Table 3 of the main article. The data density of the Bragg rod data were reduced to 1 in 10 points.

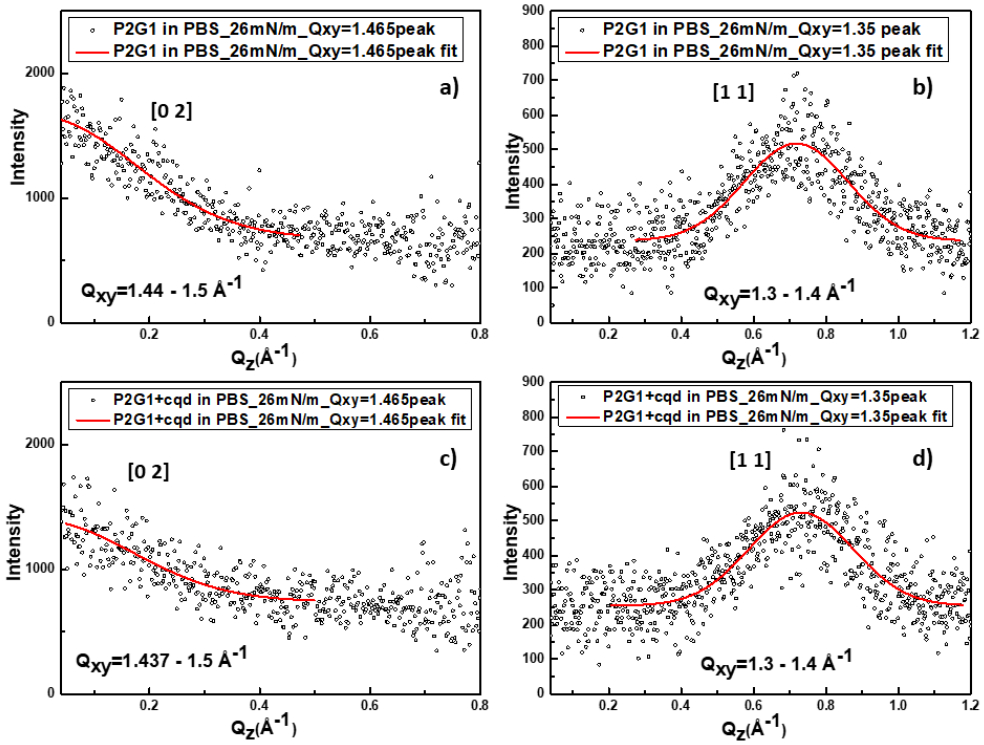

Figure 13. a) [0 2] and b) [1 1] Bragg rod profiles of pristine P2G1 on PBS subphase; c) [0 2] and d) [1 1] Bragg rod profiles of P2G1 after CQD binding.

the [1 1] rod increases in width. It implies that the ordered DPPG tails become orientationally disordered normal to the interface and there is no extra ligand layer above the FLM which validates the slab model used to fit the XR data of this system.

The Bragg peaks of the P2G1 FLM on DI water at 26 mN/m collected before and after addition of the CQDs are shown in the main article. ESI Fig. S12 illustrates the Bragg rods of the corresponding Bragg peaks. The GID data does not visibly alter after addition of the CQDs.

References:

1. A. Saha, S.K. Basiruddin, R. Sarkar, N. Pradhan and N.R. Jana, *The Journal of Physical Chemistry C*, 2009, **113**, 18492-18498.

2. S.J. Tan, N.R. Jana, S. Gao, P.K. Patra and J.Y. Ying, *Chemistry of Materials*, 2010, **22**, 2239-2247.